Wind and Structures, *Vol. 20, No. 3 (2015) 363-388*
DOI: http://dx.doi.org/10.12989/was.2015.20.3.363

Optimization of multiple tuned mass dampers for large-span roof structures subjected to wind loads

Xuanyi Zhou[1], Yongjian Lin[2] and Ming Gu[*1]

[1]*State Key Laboratory of Disaster Reduction in Civil Engineering, Tongji University, Shanghai 200092, China*
[2]*China Southern Airlines Company Limited Basic Construction Management Division, Guangzhou 510406, China*

(Received September 17, 2014, Revised November 30, 2014, Accepted January 12, 2015)

Abstract. For controlling the vibration of specific building structure with large span, a practical method for the design of MTMD was developed according to the characteristics of structures subjected to wind loads. Based on the model of analyzing wind-induced response of large-span structure with MTMD, the optimization method of multiple tuned mass dampers for large-span roof structures subjected to wind loads was established, in which the applicable requirements for strength and fatigue life of TMD spring were considered. According to the method, the controlled modes and placements of TMDs in MTMD were determined through the quantitative analysis on modal contribution to the wind-induced dynamic response of structure. To explore the characteristics of MTMD, the parametric analysis on the effects of mass ratio, damping ratio, central tuning frequency ratio and frequency range of MTMD, was performed in the study. Then the parameters of MTMD were optimized through genetic algorithm and the optimized MTMD showed good dynamic characteristics. The robustness of the optimized MTMD was also investigated.

Keywords: large-span roof; MTMD; mode contribution; optimum analysis; genetic algorithm; constrain conditions; TMD spring

1. Introduction

In recent years, some large-scale scientific instruments are installed in a laboratory with large span. Shanghai Synchrotron Radiation facility located in Pudong district of Shanghai, China, which is a scientific platform for basic researches, is such kind of modern laboratory. For the purpose of scientific research, the vibration of building structure of laboratory should be strictly controlled under external excitations including wind loads; otherwise the vibration of structures could transfer to the scientific equipment, which may reduce the accuracy of instruments. Therefore, the vibration of the important structures must be strictly under control.

As we all know, TMD is effective in restraining the vibration of some "simple" structure. The "simple" structure, such as high-rise structure, herein refers to the structure whose vibration only certain mode mainly contributes to. However, large-span roofs usually have closely spaced natural frequencies, which leads to multi-mode contribution to their structural vibration. In this situation, a single tuned mass damper (STMD) hardly shows good behavior in reducing the

*Corresponding author, Professor, E-mail: minggu@tongji.edu.cn

http://www.techno-press.org/?journal=was&subpage=8 ISSN: 1226-6116 (Print), 1598-6225 (Online)

vibration of large-span roofs. As a solution, the use of more than one TMDs with different dynamic characteristics, was proposed by Xu and Igusa (1992) to improve the effectiveness and robustness. The multiple tuned mass dampers (MTMDs) for controlling the structural vibration consist of a large number of small TMDs whose natural frequencies are distributed around the natural frequency of a controlled mode of the structure. Moreover, since MTMD is composed of several small TMDs, it is more flexible and easily manufactured than STMD in engineering practice. A single TMD in MTMD has small mass and volume, which wouldn't affect the usage of interior space of laboratory significantly. The advantages above make MTMD superior to STMD in term of the robustness and convenience when the vibration of large-span structures needs to be reduced.

Many researchers have made contributions to the study on the characteristics of MTMD. Abe and Fujino (1994) studied the modal characteristics and efficiency of the MTMD analytically. Perturbation solutions for the modal properties of the MTMD-structure system were obtained and the modal characteristics discussed. They derived an explicit formula to estimate the effectiveness of the MTMD subjected to harmonic forces. The dynamic characteristics and effectiveness of MTMD under random loading were investigated by Kareem and Kline (1995). And a parameter study was conducted to delineate the influence of several parameters on the effectiveness and robustness of MMDs in comparison with a STMD. Li and Liu (2000, 2002a) studied the performance of multiple tuned mass dampers for attenuating undesirable oscillations of structures under the ground acceleration. The numerical results indicated that for the MTMD there exist the near-zero optimum average damping ratio, invariant optimum frequency spacing, irregular change of the optimum tuning frequency ratio, deteriorating range of the effectiveness, failure ranges of the total mass ratio, and maximum allowable total number.

The distribution pattern of MTMD also attracted many attentions from scholars. In 1995, Abe and Igusa (1995) further described the coupling between the motions of the p modes of the structure and the multiple TMDs. The results showed that properly placed attachments of TMDs to the structure are important to control the response. Park and Reed (2001) numerically evaluated the performance of multiple dampers with uniformly and linearly distributed masses, respectively, under harmonic excitation. They showed that the uniformly distributed mass system is more effective in reducing the peak dynamic magnification factor. Li (2002b) conducted a study to search for the preferable MTMD which performs better and is easily manufactured. These MTMD comprised various combinations of the stiffness, mass, damping coefficient and damping ratio in the MTMD. The double tuned mass dampers (DTMD), consisting of one larger TMD and one smaller TMD, was further proposed by Li and Zhu (2006a) to seek for high effectiveness and robustness for the reduction of the undesirable vibrations of structures under the ground acceleration. Carneiro *et al*. (2008) numerically investigated the dynamic performance of a controlled high-rise building. In the paper, the effects of different numbers of mass dampers and their interconnection were considered.

Except for researches on the basic characteristics of MTMD, investigations on the engineering application of MTMD also have been reported. Zheng *et al*. (2002), Avila and Goncalves (2009), Lewandowski and Grzymislawska (2009), Moon (2010), Patil and Jangid (2011) studied the application of MTMD in high-rise buildings. Jangid and Datta (1997), Singh *et al*. (2002), Ahlawat and Ramaswamy (2003), Wang and Lin (2005), Li and Qu (2006b), and Desu *et al*. (2006) explored the dynamic characteristics of MTMD on torsionally coupled structures. Gu *et al*. (2001), Chang *et al*. (2003), Chen *et al*. (2003), Kwon and Park (2004) and Ubertini (2010) discussed the effectiveness of MTMD in wind-induced response vibration control of long-span bridge. Carpineto

et al. (2010), Li *et al*. (2010) and Daniel *et al*. (2012) applied the MTMD to reduce the pedestrian-induced vibration of footbridge. Hwang *et al*. (2011) and Nguyen *et al*. (2012) controlled the floor vibration using MTMD.

However, compared with high-rise structures and long-span bridges, it is more difficult for large-span structures to get placement and optimal parameters of MTMD due to its characteristics of three-dimensional effect, closely spaced natural frequencies. Few researches concerning the application of MTMD in structures with closely spaced natural frequencies have been reported yet. In the present study, the optimization method of MTMD for large-span roof structures subjected to wind loads was established. In the method, the dynamic characteristics of wind-induced response of large-span roofs were used to determine the controlled modes and placements of TMDs in MTMD. Moreover, as an important pre-condition in engineering practice, the strength and fatigue life of TMD spring were involved as the constraint condition during the process of optimization. To examine the efficiency of MTMD, the new method was applied to a specific shell structure. And the control effect, effect of TMDs spring constraints and robustness of MTMD were evaluated.

2. Analytical model of structures with MTMD

2.1 Numerical simulation procedure

The dynamic equation of structure-MTMD model was (Connor 2003)

$$[M_S]\{\ddot{x}_S\}+[C_S]\{\dot{x}_S\}+[K_S]\{x_S\}=\{F(t)\}-[H]\{U(t)\} \tag{1}$$

$$[M_T]\{\ddot{\upsilon}\}+[C_T]\{\dot{\upsilon}\}+[K_T]\{\upsilon\}=-[M_T][H]^T\{\ddot{x}_s\} \tag{2}$$

$$\{U\{t\}\}=\begin{Bmatrix} -c_{t1}\dot{\upsilon}_{t1}-k_{t1}\upsilon_{t1} \\ \vdots \\ \vdots \\ -c_{tm}\dot{\upsilon}_{tm}-k_{tm}\upsilon_{tm} \end{Bmatrix} \tag{3}$$

where $[M_s]$, $[C_s]$ and $[K_s]$ are the mass, damping and stiffness matrixes of the main structure, which are $n\times n$ (n is the total degree of freedom (DOF) of the main structure) dimensional matrixes. $\{x_s\}$, $\{\dot{x}_s\}$ and $\{\ddot{x}_s\}$ are the displacement, velocity and acceleration vectors of the main structure respectively, which are n-dimensional vectors. $\{F(t)\}$ is the fluctuating wind load (a n-dimensional vector) on the structure. $\{U(t)\}$ is the MTMD control force vector (a m-dimensional vector; m is equal to the total number of MTMDs). $[H]$ is a $n\times m$ dimensional MTMD placement matrix, which is composed of 0 and 1. H_{kj} =1 means that TMD j is installed on the DOF k. $[M_T]$, $[C_T]$ and $[K_T]$ are the mass, damping and stiffness matrixes of the MTMD, which are $m\times m$ dimensional matrixes respectively. $\{\upsilon\}$, $\{\dot{\upsilon}\}$ and $\{\ddot{\upsilon}\}$ are the displacement, velocity and acceleration vectors of TMD relative to the main structure respectively, which are m-dimensional vectors.

The power spectra of generalized displacement of structure and relative displacement of MTMD can be gained using the knowledge of structural dynamics and random vibration

$$[S_{RR}(\omega)] = [\Phi][S_{qq}(\omega)][\Phi]^T \tag{4}$$

where $[\Phi]$ is the matrix of the structural mode, and $[S_{qq}(\omega)]$ is the power spectrum of generalized displacement of the structure.

When the power spectrum wind loads is a unilateral spectrum, the root mean square (RMS) of structural displacement is

$$\sigma_R = \sqrt{\int_0^\infty S_{RR}(\omega)d\omega} \tag{5}$$

The peak response of structural displacement is defined as

$$P = \overline{R} \pm \overline{g}\sigma_R \tag{6}$$

where $\overline{R}$ is the mean response of structural displacement, σ_R is the RMS of structural displacement and $\overline{g}$ is a peak factor, valued 2.5 in this paper.

The reduction factor of dynamic response is defined as

$$R_\sigma = 1 - \sigma_w / \sigma_0 \tag{7}$$

where σ_0 and σ_w are the values of RMS of structural displacement before and after the integration of MTMD, respectively. Larger reduction factor represents better control effect.

The mean reduction factor is defined as

$$\overline{R} = \frac{\sum_{i=1}^{N} R_{\sigma i}}{N} \tag{8}$$

where N is the total number of concerned structural responses and $R_{\sigma i}$ is the reduction factor corresponding to response i.

2.2 Constraint conditions of TMDs

Since TMDs are subjected to fluctuating wind load during their service life, the strength and fatigue life of TMD spring have to satisfy the usage requirements. And the problem of TMD springs' fatigue life is vital. During the optimization of MTMD, the constraint conditions for strength and fatigue life of TMD spring were taken into account by referring to the method of Gu and Xiang (1992).

Given the mass and natural frequency of TMD, its stiffness can be determined

$$k_T = m_T \omega_T^2 \tag{9}$$

where m_T is the mass of TMD, determined by the mass ratio of TMD; ω_T is the circular

frequency of TMD, determined by the central tuning frequency of TMD. The static displacement of spring would be produced under the dead weight of TMD

$$Y_0 = \frac{m_T g}{k_T} = \frac{g}{\omega_T^2} \tag{10}$$

where g is the gravitational acceleration (9.8m/s^2).

When TMD vibrates, its dynamic response is $Y_\sigma = \bar{g}\sigma_T$, where $\bar{g}$ is a peak factor valued as 2.5 and σ_T is the RMS of dynamic displacement of TMD. Then, the peak displacement of TMD's spring is

$$Y = Y_0 \pm Y_\sigma = g/\omega_T^2 \pm \bar{g}\sigma_T \tag{11}$$

Then, the requirement for strength of TMD spring (Design of cylindrical helical springs, 2009) is below

$$KG\left(\bar{g}\sigma_T + g/\omega_T^2\right)/\left(\pi C^2 H\right) - [\tau] \leq 0 \tag{12}$$

where $[\tau]$ is the allowable shearing stress of spring material, G is shear modulus of spring material, $H = nd$ is the free length of spring, n is the effective coil number of spring, d is the diameter of spring wire, curvature correction factor $K = \left[0.615/C + (4C-1)/(4C-4)\right]$, the spring index is $C = D/d$, and D is the mean diameter of coil.

And the requirement for fatigue strength considering the vibration of TMD's spring (General Administration of Quality Supervision, Inspection and Quarantine of the People's Republic of China, Standardization Administration of the People's Republic of China, 2009a) is

$$\tau_0 - \left[(S_F - 0.75)\, g/\omega_T^2 + (S_F + 0.75)\bar{g}\sigma_T\right] KG/\left(\pi C^2 H\right) \geq 0 \tag{13}$$

where τ_0 is shearing fatigue limit of spring material under pulsation shearing stress and S_F is the design safety factor of fatigue strength of spring.

2.3 Optimization of MTMD

2.3.1 Optimization object function

The optimization object function has to be set during the optimization of MTMD. Although, MTMD is to control the structural displacement response in this paper, the controlled objects can be conveniently changed into other types of response, such as acceleration, stress of rod and support reaction. Thus, the method proposed herein is universally applicable for the effect of different types of optimization object function wasn't discussed here. This paper took the sum of RMS of displacement at all TMD placements as the optimization object function

$$f_{opt} = \sum_{i=1}^{n} \sigma_i \tag{14}$$

where n is the total number of TMDs and σ_i is the RMS of vertical structural displacement response at TMD i.

2.3.2 Genetic algorithm

Many optimization algorithms have been proposed by researchers. For it is not the focus of the study, genetic algorithm (GA) was chosen herein as optimization optimization (Beasley *et al*. 1993). In this paper, the global optimization of GA, which is provided by MATLAB, was used to optimize the parameters of MTMD.

3. Research object and description of wind tunnel test

3.1 Research object

A 6×24 monolayer reticulated spherical shell was taken as the research object. The spherical shell is made up of radial ribs and ring bars. The radial ribs intersect in the top center of shell. Its span L is 40.0 m and the rise-span ratio f is 1/6. This type of structure is widely used for many kinds of large-span roofs, such as laboratory, industrial factory building, stadium.

3.2 Wind tunnel test

In order to compute the dynamic responses of the roof, the fluctuating wind pressures acting on the roof were obtained from a wind tunnel test. The test was carried out in TJ-2 Boundary Layer Wind Tunnel in Tongji University, whose working section is 3.0 m wide and 2.5 m high. The objective wind field of the terrain category B in accordance with the Chinese Code (Load code for the design of building structures, 2012) was simulated with a standard spire-roughness arrangement on the wind tunnel floor. The exponent of the mean wind speed profile was 0.15. The geometry scale was 1:150. Reference wind speed at the height of 1.0 m (equivalent to 150.0 m high in the atmospheric boundary layer) in the wind tunnel for the measurement obtained from the pitot tube was 12.0 m/s, and the wind velocity UH at the height of the model's roof top (H=0.20 m) was 9.43 m/s, indicating that the velocity scale was 1:3.71. And the turbulence intensity of roof top was 15%. The wind pressures at 127 measuring points, which were distributed evenly on the roof surface, were simultaneously measured on the rigid model of the roof. The pressure taps were connected with the measurement system through PVC tubing. To avoid the distortion of the dynamic pressure, the signals had been modified using the transfer function of the tubing systems. The pressure signals were sampled at 312.5 Hz. The detailed description of characteristics of wind pressure on the roof surface can be found in the reference (Lin 2013).

4. Wind-induced response and determination of controlled modes and placements of TMDs

4.1 Modal analysis

The dynamic behaviors of the roof structure are computed before the computation of the wind induced responses. Fig. 1 presents the first twelve mode shapes and the corresponding natural frequencies of the structure. The first natural frequency is 0.805 Hz, and about 12 mode shapes range from 0.80 to 0.90 Hz. The natural frequencies are found to be fairly close to one another. This is a very important consideration when analyzing the dynamic response of large-span roofs.

Since the reticulated shell has a symmetric structure, the mode shapes also have symmetric characteristics. The first and second mode shapes vibrated horizontally along X and Y axis, while the third mode shape rotated around the Z axis.

4.2 Characteristics of wind-induced response

The wind-induced responses of the structure without MTMD were calculated by using the abovementioned frequency domain method. The basic wind pressure was 0.55kPa and the structural damping ratio ξ was 0.01. The number of mode participating in vibration was 100.

For the convenience of description, the structure was divided into five rings (R0-R4) from inside to outside (shown in Fig. 2). The points with maximum wind-induced vibration of these five rings under 0° wind direction were pointed out, presented as P0-P4 in Fig. 2.

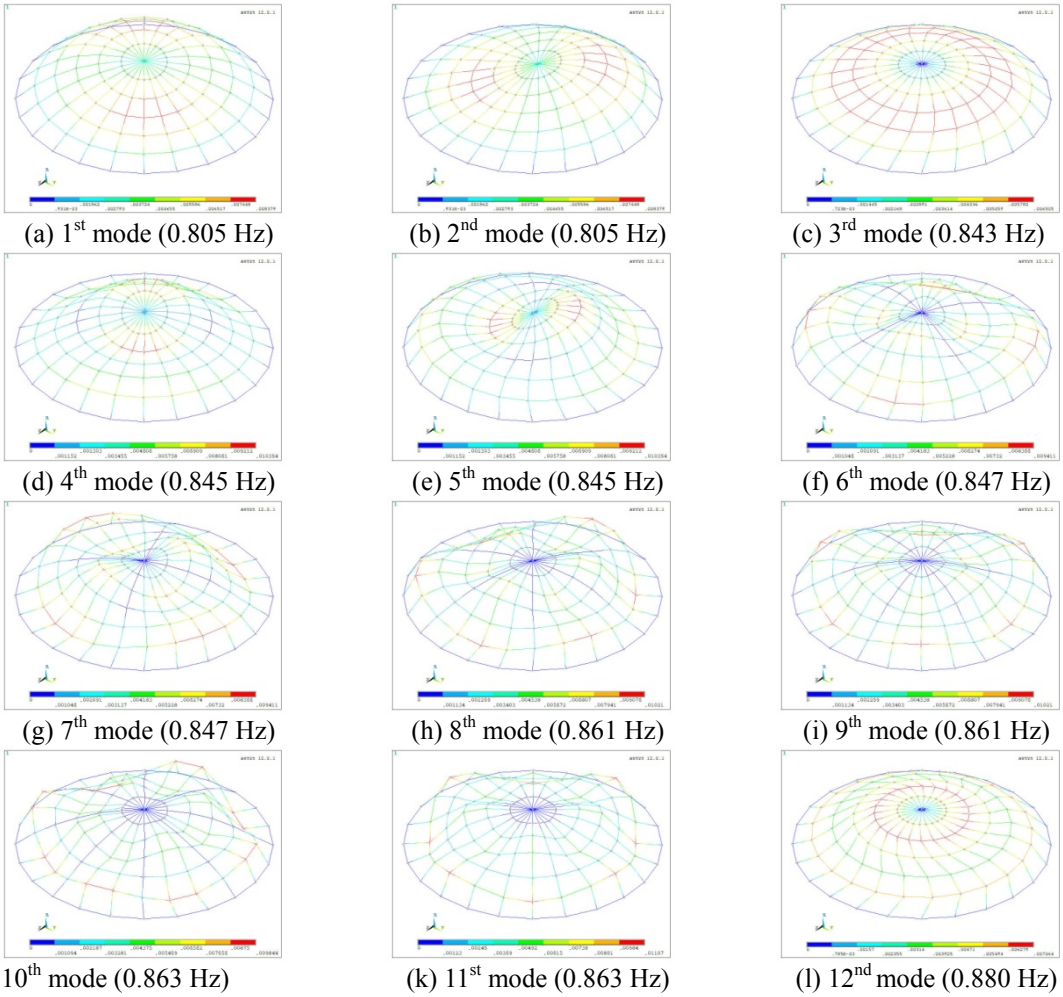

(a) 1st mode (0.805 Hz) (b) 2nd mode (0.805 Hz) (c) 3rd mode (0.843 Hz)

(d) 4th mode (0.845 Hz) (e) 5th mode (0.845 Hz) (f) 6th mode (0.847 Hz)

(g) 7th mode (0.847 Hz) (h) 8th mode (0.861 Hz) (i) 9th mode (0.861 Hz)

(j) 10th mode (0.863 Hz) (k) 11st mode (0.863 Hz) (l) 12nd mode (0.880 Hz)

Fig. 1 Typical mode shapes and natural frequencies

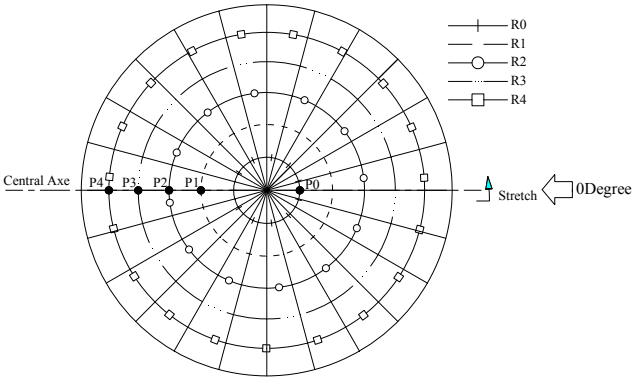

Fig. 2 Nodes of maximum wind-induced responses of different rings

The calculation results demonstrated larger vertical displacement response along with Z axis compared to horizontal responses. Thus, the peak and RMS of displacement response of counterclockwise distributed nodes along the arrow in Fig. 2 were presented in Fig. 3. Node NO. in the abscissa shows the position of node. NO. 1 presents the starting point in the stretch arrow (shown in Fig. 2), and the number increases anticlockwise. It can be known from Fig. 3(a) that the vertical displacement response of the structure could reach as high as to 12.8 cm, indicating larger structural response. According to Fig. 3(b), the maximum wind-induced vibration of five rings occurred on P0, P1, P2, P3 and P4, respectively. P0 was close to the reticulated shell center on the windward side, whereas P1-P4 located at the central axis of roof on the leeside. R1 achieved the largest dynamic response, followed by R4, R2, R3 and R0 successively. For targeting at the reduction of wind-induced vibration, this paper only focused on rings with large wind-induced vibrations. Since ring R0 showed significantly smaller wind-induced vibrations than rest rings, this paper only analyzed the characteristics of wind-induced vibrations of R1, R2, R3 and R4.

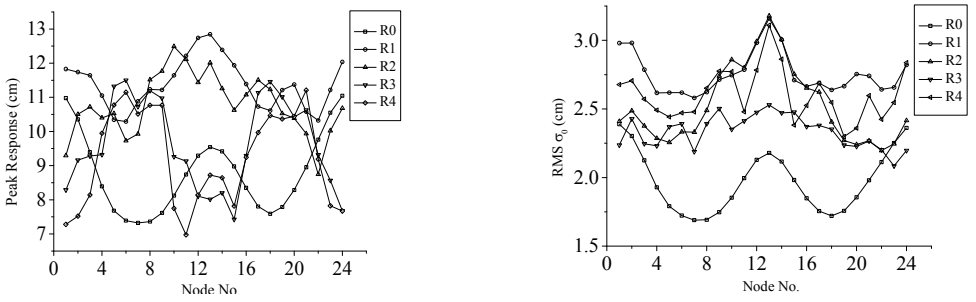

(a) Peak responses of nodes on each ring (b) Displacement RMS of nodes on each ring

Fig. 3 Wind-induced responses

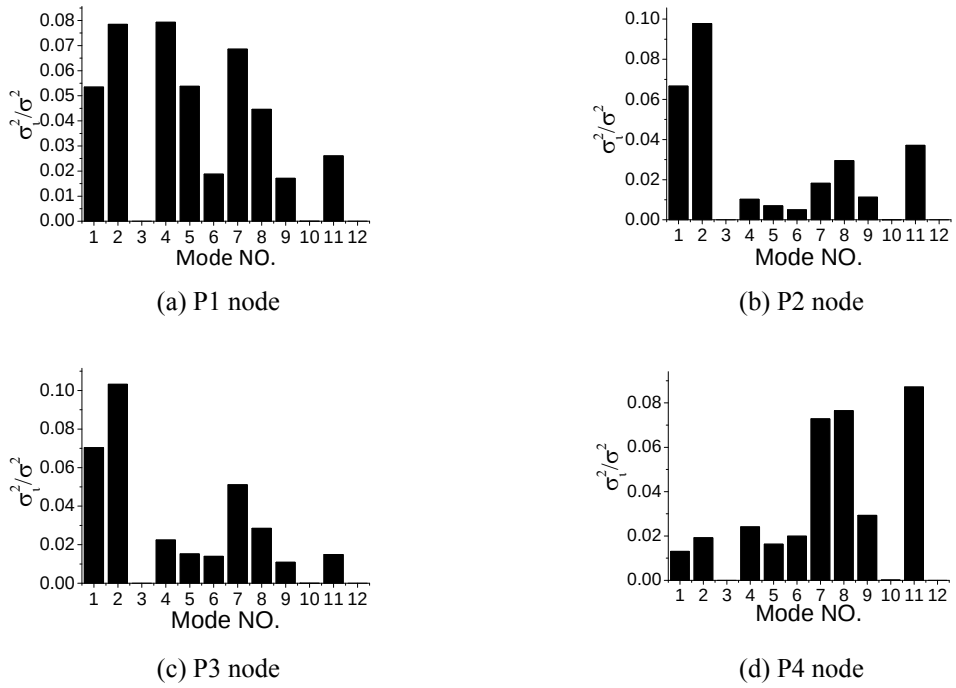

(a) P1 node (b) P2 node

(c) P3 node (d) P4 node

Fig. 4 Modal contribution to resonant response

Since MTMD can control the resonant component of wind-induced dynamic response, the mode contributions to resonant component, which is shown in Fig. 4, were analyzed by using the method proposed by Zhou and Gu (2010). Fig. 4 presents that, different nodes produced great vibrations at multiple natural frequencies, showing characteristics of typical multi-modes coupled effects. For different nodes, modes made significant different contributions to resonant component. The nodal displacement at P1 brought great contributions (8%) of 2nd and 4th modes to resonant component. Larger resonances were also observed at P1 under other modes. Node P2 mainly produced resonances at the 1st and 2nd natural frequencies. The modal contribution of the second mode even reached to 10%. Node at P3 showed similar vibration with that at P2, that is, resonances were mainly produced at the first and second natural frequencies. At P4, resonances were mainly contributed by the 7^{th}, 8^{th} and 11^{st} modes, each of which showed a modal contribution of more than 7%. For the symmetry of the roof structure, the characteristics mentioned above at P1-P4 can represent the vibration characteristics of their corresponding rings. The results of modal analysis showed the same value of 1st and 2nd natural frequencies, 4th and 5th natural frequencies, as well as 8th and 9th natural frequencies. Additionally, the points with larger displacement at 1st and 2nd modes as well as 4th and 5th modes were basically within ring R1 where node P1 lies in. As a result, the maximum resonant energy of R1 was believed to be at the natural frequencies 0.805 Hz, 0.845 Hz. Similarly, the maximum resonant energy of R2 and R3 were believed at 0.805 Hz. The R4 was relative complicated as 7^{th}, 8^{th} and 11^{st} natural frequencies all made great modal

contributions to the resonant response. Thus, 0.861 Hz for the 8th natural frequencies, which located in the middle position, was chosen as the controlled frequency for ring R4.

4.3 Controlled modes and placements of TMDs

According to the analysis on the characteristics of wind-induced response, the resonant component of vibration is very complicated associated with the effects of multi-modes coupled vibrations and different responses have different resonant frequencies contributing most of energy. Hence, the following would set controlled frequencies and placements of TMDs of the MTMD according to the response characteristics of rings. No TMDs was set in ring R0 due to its small vibration. Each of the rest four rings were equipped with different groups of MTMDs, numbered as G1, G2, G3 and G4. G1 is used to control R1, G2 for R2, G3 for R3 and G4 for R4.

The controlled frequencies of MTMDs were the natural frequencies of modes with maximum contributions to resonant component. As mentioned before, the natural frequency with maximum mode contribution of R2 was 0.805 Hz, so the controlled frequency and modes of G2 were 0.805 Hz, 1st and 2nd modes respectively. The maximum resonant energy of G1 was found at the natural frequencies 0.805 Hz, 0.845 Hz. Since the controlled frequency of G2 and G3 was set as 0.805 Hz, the controlled frequencies and modes of G1 was determined as 0.845 Hz, 4th and 5th modes respectively. Thus, the controlled frequencies, modes and corresponding rings of four MTMD groups were listed in Table 1.

Placement and number of TMD are also important parameters for MTMD. With three-dimensional effect, it is more difficult for large-span structure to analyze the effect of TMD placement and number on the control effect compared with high-rise structure. Therefore, the placement and number of TMD were determined according to the key nodes with large displacement in the controlled modes according to Table 1.

The key nodes with large displacement of different vibration modes can be easily pointed out by analyzing the mode shapes carefully in Fig. 1. Fig. 5 presented the positions of the key nodes, which were used to determine the placement of the MTMDs. As mentioned before, G1 controls R1 and the control frequency is 0.845 Hz, the position of TMDs in G1 were determined according to Fig. 5(a). Similarly, the placements of other MTMDs can be determined.

The placement of TMDs were summarize to been shown in Fig. 6, where G1-G3 were composed of 16 TMDs respectively, and G4 was composed of 12 TMDs.

Table 1 Controlled ring and tuning frequency of four MTMD groups

NO. MTMD	controlled ring	controlled modes	tuning frequency (Hz)
G1	R1	4、5	0.845
G2	R2	1、2	0.805
G3	R3	1、2	0.805
G4	R4	8	0.861

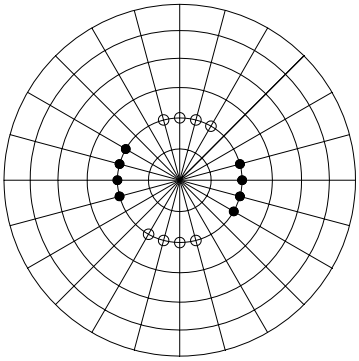

(a) Key nodes of 4th and 5th modes on R1

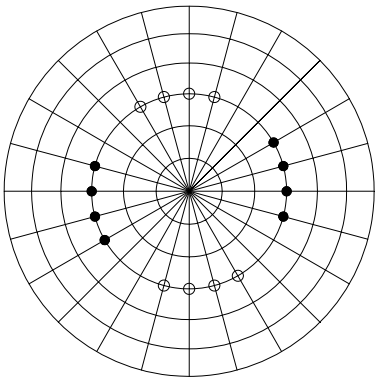

(b) Key nodes of 1st and 2nd mode on R2

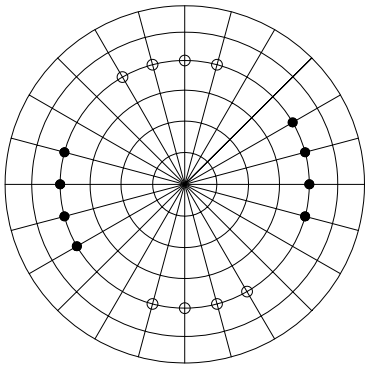

(c) Key nods of 1st and 2nd mode on R3

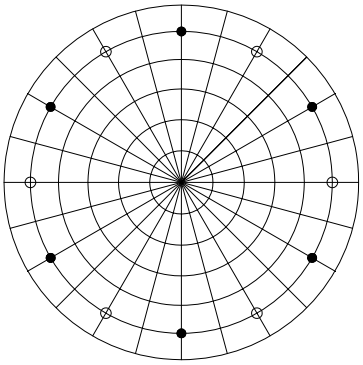

(d) key nodes of 8th and 9th mode on R4

Fig. 5 Key nodes of controlled modes on each ring

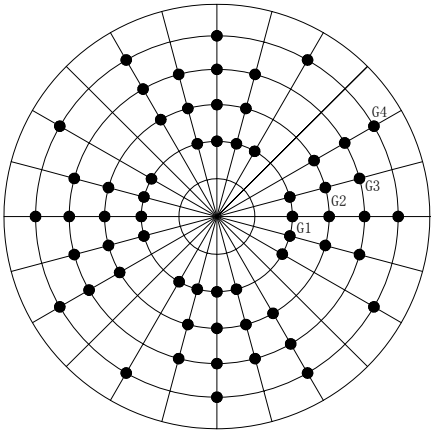

Fig. 6 Position of TMDs

Table 2 Parameters of MTMD in parametric study

total mass ratio (μ)	damping ratio (ξ_T)	central tuning frequency ratio (λ)	frequency range (β) /Hz
2.0 %	7%	1.0	0.08

5. Parametric analysis of MTMD

Due to the complexity of MTMD, parametric analysis on control effect of MTMD was performed firstly, which provided initial range of parameters for subsequent optimization. The following parametric analysis mainly focused on the mass ratio, damping ratio, central tuning frequency ratio and frequency range of MTMD. To explore the vibration control effects of MTMD parameters, the analysis of one parameter was conducted under the precondition of fixed values of other parameters. The fixed values of parameters were determined according to the following principle.

Abe and Fujino (1994) carried out parametric analysis under 1%~2% for MTMD mass ratio. Hecne, when analyzing other parameters, the total MTMD mass ratio was determined 2%, and the total MTMD mass was distributed evenly to four MTMD groups, that is, 0.5% for each group. Meanwhile, every TMD has equal mass.

After the total MTMD mass ratio was determined, the damping ratio was calculated 7% using Warburton's (1982) theoretical formula $\frac{1}{2}\sqrt{\frac{\mu(1+3\mu/4)}{(1+\mu)(1+\mu/2)}}$,where μ is mass ratio. Therefore, damping ratio was determined as 7% when analyzing other parameters.

The central tuning frequency ratio was calculated from Den Hartog's(1956) optimal frequency ratio formula for undamped structure ($\lambda = \frac{1}{1+\mu}$). In this paper, the central tuning frequency ratio was determined 1.0 when analyzing other parameters because of the multi-mode effects on dynamic vibration.

Abe and Fujino (1994) proposed the theoretical formula of minimum frequency range of MTMD. Based on this formula, the minimum frequency range in this paper of MTMD was determined as 0.08 Hz when analyzing other parameters.

The values of MTMD parameters for parametric analysis were summarized in Table 2.

5.1 Effect of total mass ratio

Fig. 7 showed the relationship between the total mass ratio and vibration reduction factor as well as the relationship between the total mass ratio and mean vibration reduction factor of G1-G4. In the figure, the curves with hollow marks for P1-P4 denote the reduction factor for single nodes defined by Eq. (7), whereas the curves with solid marks for G1-G4 denote the mean reduction factor for different rings defined by Eq. (8). It demonstrated that larger MTMD mass ratio would bring larger vibration reduction factor. However, after the total mass ratio reached the certain value (1.6%), such growth of vibration reduction factor slowed down with the continuous increasing of mass ratio. Furthermore, the best vibration control effect was observed on P4. Different MTMD groups showed different control effect and G1 achieved the best.

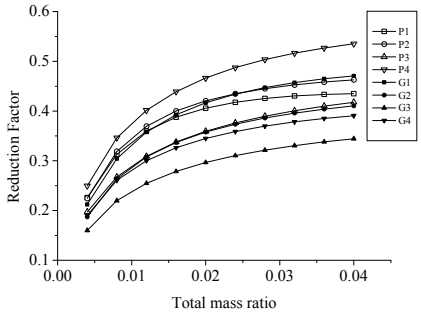

Fig. 7 Effect of total mass ratio on reduction factor

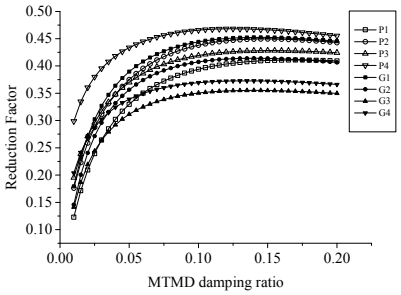

Fig. 8 Effect of MTMD damping ratio on reduction factor

5.2 Effect of damping ratio

The relationship between the MTMD damping ratio ξ_T and vibration reduction factor was represented in Fig. 8. The reduction factor and mean reduction factor of different MTMD groups changed similarly with the damping ratio of TMDs. When the damping ratio of TMD was smaller than 0.05, the reduction factor increased quickly with the increasing of damping ratio. However, the vibration reduction factor increased slightly with the further increasing of damping ratio. This indicated that all MTMDs have an optimal damping ratio. According to Fig. 9, the optimal damping ratio of MTMD was ranging from 7% to 12%.

5.3 Effect of central tuning frequency ratio

Fig. 9 represented the relationship between the central tuning frequency ratio and reduction factor. Both the reduction factors at a single node and mean reduction factors have different optimal central tuning frequency ratios. Meanwhile, different reduction factors have different sensitivities to the central tuning frequency ratio. Compared with other nodes, P4 is most sensitive to the central tuning frequency ratio. According to Fig. 9, the reduction factor at a single node is more sensitive to the change of central tuning frequency ratio than the mean reduction factor. The optimal central tuning frequency ratio of G1 and G4 was about 0.98, whereas that of G2 and G3 was about 1.05.

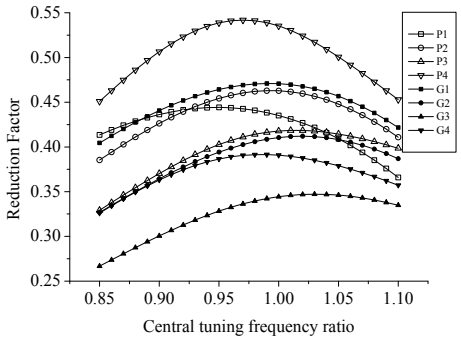

Fig. 9 Effect of central tuning frequency ratio on reduction factor

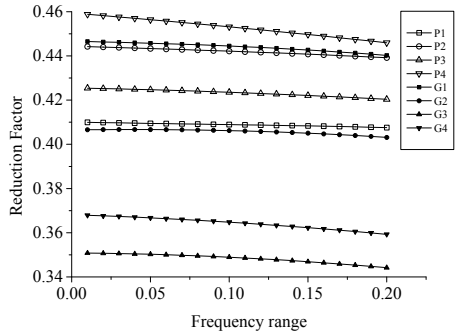

Fig. 10 Effect of frequency range on reduction factor

5.4 Effect of frequency range

Fig. 10 represented the relationship between the frequency range and vibration reduction factor, showing a slight decrease of the reduction factor with the increasing of frequency range. The reduction factor of P4 decreased relatively obviously with the increasing of frequency range. In a word, no great effect of frequency range was observed on the control effects of MTMDs. Therefore, the requirement of frequency range of MTMDs can be relaxed appropriately to increase its robustness.

5.5 Effect of mass distributed of different MTMD groups

The effect of five different mass distributions for four MTMD groups (shown in Table 3) was discussed under the fixed total MTMD mass ratio (2%). Fig. 11 is the histogram of reduction factors of P1-P4 and mean vibration reduction factors of G1-G4 under five different mass distributions. When the mass ratio of MTMD increased, the reduction factors of single nodes and mean reduction factors of rings also increased, which agrees with above analysis result that larger mass ratio would bring larger reduction factor.

Table 3 Mass proportions of four MTMD groups

NO. Case	G1	G2	G3	G4
Case 1	25%	25%	25%	25%
Case 2	55%	15%	15%	15%
Case 3	15%	55%	15%	15%
Case 4	15%	15%	55%	15%
Case5	15%	15%	15%	55%

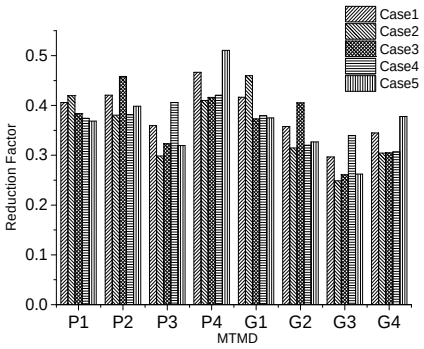

Fig. 11 Effect of different mass proportions of MTMD groups on reduction factor

6. Parameter optimization of MTMDs

Based on the results of parametric study above, the optimal parameters of four MTMD groups were calculated through the global optimization toolbox of GA of Matlab.

6.1 Optimization constraints

The MTMD control system includes four MTMD groups. Each MTMD group has four parameters: mass ratio, damping ratio, central tuning frequency ratio and frequency range, so there are 16 parameters have to be optimized. To improve the efficiency of optimization, the upper and lower limit of optimal parameters were determined according to the results of parametric analysis above. Meanwhile, the same parameters of different MTMD groups were required to have the same upper and lower limit.

As stated before, the growth of reduction factor slowed down with the continuous increasing of total MTMD mass ratio when reached a certain value. Based on the results of parametric study, the upper limit of total MTMD mass ratio was determined 1.6%, that is, $\sum_{i=1}^{4}\mu_i = 1.6\%$, where μ_i is the mass ratio of G. During the parameter optimization, the Mass proportion of four MTMD groups was allocated by the optimization program. If the total MTMD mass ratio is too large, the weight of TMDs will cause negative effect on the structure. Therefore, the static displacement

response of the structure under the dead weight of MTMD was analyzed in this paper. The maximum vertical static displacement caused by the weight of MTMD under different total mass ratios was listed in Table 4. It can be known from Table 4 that larger total MTMD mass ratio would produce larger response. When the total MTMD mass ratio reached 1.6%, the maximum displacement caused by the weight of MTMD was only 1.28 cm, which was insignificant to the structure.

According to the results of parametric analysis, the optimal damping ratio of MTMD was 7%~12%. During the optimization, this range was expanded to 5%~20% in considering of the effect of mass ratio.

From the results in Section 4, the optimal central tuning frequency ratio of MTMD was ranging 0.98~1.05. This paper expanded it to 0.9~1.1 in considering of its potential drift for optimization.

Section 4 concluded that the frequency range of MTMD was insignificant to the control effect and suggested to relax the frequency range of MTMD appropriately in order to increase its robustness. To prevent MTMD from being changed into multiple STMDs, the frequency range would not be over wide (Abe and Fujino 1994). In addition, for the major energy of excitation ranged between 0.8~0.9 Hz, the frequency range of MTMD was finally determined between 0.08 Hz~0.2 Hz.

6.2 Results of optimization

6.2.1 Optimized parameters

Optimized results of MTMD's parameters without involving spring constraints were listed in Table 6. Different MTMD groups have different mass ratios: G1>G2>G4>G3. According to the results in Section 4, given a fixed total mass ratio, the MTMD group with higher proportion of mass ratio achieved better control effect. Hence, during the optimization targeting at minimum sum of RMS of displacement at all TMD placements, mass ratio of MTMD is surely related with the vibration strength and TMD number of the corresponding control ring. According to the wind-induced vibration analysis, R1 achieved the largest dynamic response, followed by R4, R2 and R3 successively, which basically agrees with the optimal mass distribution of corresponding rings. Furthermore, the optimized mass ratio of G2 is found slightly larger than that of G4. This was due to R2 includes 16 TMDs but R4 only 12 TMDs, though R4 has slightly larger dynamic response than R2.

Table 4 Maximum static displacement of structure under different total mass ratios

Total mass ratio	0.4%	0.8%	1.2%	1.6%	2.0%	2.4%	2.8%
Maximum static displacement (cm)	0.34	0.69	1.03	1.38	1.72	2.07	2.41

Table 5 Upper and lower limit of MTMD parameters for optimization

	total mass ratio (μ)	damping ratio(ξ_T)	central tuning frequency ratio (λ)	frequency range (β) /Hz
upper limit	1.6%	20%	1.1	0.2
lower limit	0%	5%	0.9	0.08

Table 6 Optimized results of MTMD groups

NO. MTMD	mass ratio (μ)	damping ratio(ξ_T)	central tuning frequency ratio (λ)	frequency range (β) /Hz
G1	0.52%	9.54%	0.993	0.08
G2	0.40%	9.07%	1.068	0.08
G3	0.31%	8.92%	1.088	0.08
G4	0.37%	7.90%	0.999	0.08

Table 7 Reduction factors of P1-P4 and mean reduction factors of G1-G4

P1	P2	P3	P4	G1	G2	G3	G4
40.06%	39.70%	34.38%	43.59%	41.37%	37.26%	31.86%	28.92%

The optimized damping ratio of each MTMD group agrees with its results of parametric analysis. And the optimized damping ratios of all MTMD groups fell within 7%~12% (Section 4), indicating the reliability of the optimal damping ratio.

The optimized central tuning frequency ratio of MTMD groups disagrees a little with the results of parametric analysis. According to Section 4, the optimal central tuning frequency ratio of G1 and G4 was about 0.98, and that of G2 and G3 was about 1.05. However, Table 6 showed that the optimal central tuning frequency ratios of G1 and G4 were 0.993 and 0.999 respectively, whereas those of G2 and G3 were 1.068 and 1.088 respectively. The optimal central tuning frequency ratios of G1, G2 and G4 were close to the parametric analysis results, but that of G3 was larger than the value of parametric study. Such disagreement was caused by the different mass ratio of MTMD group between the parameter optimization and parametric analysis. In parametric analysis, mass ratio of all MTMD groups was determined 0.5%, but the optimized mass ratios were different. Particularly, the mass ratio of G3 was only 0.31%, which is 0.19% less than the result of parametric analysis. Based on the theoretical formula of optimal central tuning frequency ratio (Den Hartog 1956), smaller mass ratio of TMD would bring larger optimal central tuning frequency ratio, thus resulting in the larger optimal central tuning frequency ratio of G3.

To minimize the optimization object function, the optimal frequency range of all MTMD groups was taken the lower limit (0.08 Hz), because the reduction factor decreased with the expansion of frequency range (seen in Section 4).

6.2.2 Control effect

The power spectra of vertical displacement at P1-P4 without/with MTMD were presented in Fig. 12. The figure demonstrated the effectiveness of MTMD in lowering the resonant energy. Thus, the dynamic responses were also reduced significantly.

The reduction factors of P1-P4 and mean vibration reduction factors of G1-G4 in the optimal

MTMD were listed in Table 7. The reduction factors at P1-P4 reached more than 34% and the mean vibration reduction factors more than 28%. This indicated the good control effect of the optimized MTMD.

6.3 Effect of TMDs spring constraints

6.3.1 TMDs spring constraints

During the optimization, since spring stiffness changes with the mass ratio and frequency ratio of single TMD, the mean diameter of coil (D), diameter of spring wire (d), spring index (C=D/d) and free length of spring (H) are determined by mass ratio and frequency ratio. For the convenient implementation of spring constraint, the values of D and d were set fixed. The designed spring stiffness was maintained same with that for optimization by adjusting H. Based on this idea, the free length of spring H can be calculated from (General Administration of Quality Supervision, Inspection and Quarantine of the People's Republic of China, Standardization Administration of the People's Republic of China, 2009a),

$$H = \frac{Gd^2}{8C^3 k_T} = \frac{Gd^2}{8C^3 m_T \omega_T^2} \tag{15}$$

Values of variables in the spring constraints can be determined according to associated codes (General Administration of Quality Supervision, Inspection and Quarantine of the People's Republic of China, Standardization Administration of the People's Republic of China, 2009a, b, c, Mott 2013). The spring material used DH-type cold-drawn non-alloy steel wire for springs and the allowable tensile strength $\sigma_B = 1400$ MPa. The number of loading cycles was N≥10^7, indicating the infinite fatigue life of spring with a shearing fatigue limit under pulsation shearing stress (τ_0) of $0.35\sigma_B$. Values of spring parameters were given in Table 8. Under this circumstance, both allowable shearing stress of the spring material ($[\tau]$) and τ_0 were 490 MPa. After spring parameters were determined, H can be calculated from Eq. (15). Then, the process of optimization can be controlled by substituting these spring parameters into Eqs. (12) and (13).

6.3.2 Response of TMDs spring under different wind velocities without involving spring constraints

When the basic wind pressures are 0.35 kPa, 0.45 kPa and 0.55 kPa respectively, a preliminary study on the results of TMD optimization was conducted. The conditions of these basic wind pressures are equivalent to those with wind velocities 24 m/s, 27 m/s and 30 m/s at 10 m high above the ground respectively. In this section, the optimization neglected the effect of spring constraints. Strictly speaking, the joint probability density function between wind direction and wind velocity should be involved when dealing with the problem of fatigue.

Fig. 13 presented the RMS displacement of different TMDs at three levels of wind velocity. In the figure, TMD NO. 1-16 on the abscissa represents TMDs in G1; 16-32 represents TMDs of G2; 33-48 represents TMDs of G3; 49~60 represents TMDs of G4. The maximum shearing stress and fatigue pulsation shearing stress of TMD springs at three levels of wind velocity were shown in Figs. 14 and 15. From these figures it can be seen that, larger wind velocity is accompanied with larger vibration displacement of TMDs and larger spring stress. Such increased spring stress would increase the maximum shearing stress and fatigue pulsation shearing stress of the TMDs springs.

Table 8 Values of spring parameters

G(GPa)	σ_B (MPa)	$[\tau]$ (MPa)	τ_0 (MPa)	D(mm)	d(mm)	C(D/d)	n_F
78.5	1400	$0.35\sigma_B$	$0.35\sigma_B$	88	11	8	1.7

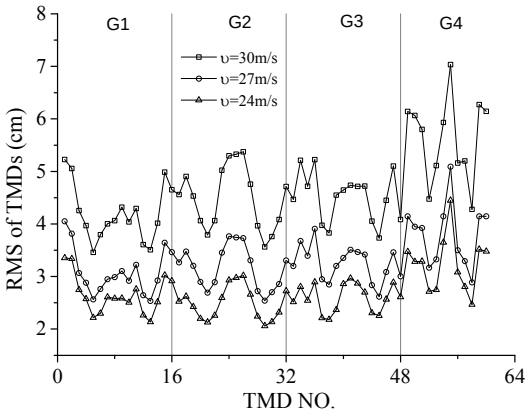

Fig. 13 RMS displacement of TMDs at three levels of wind velocity

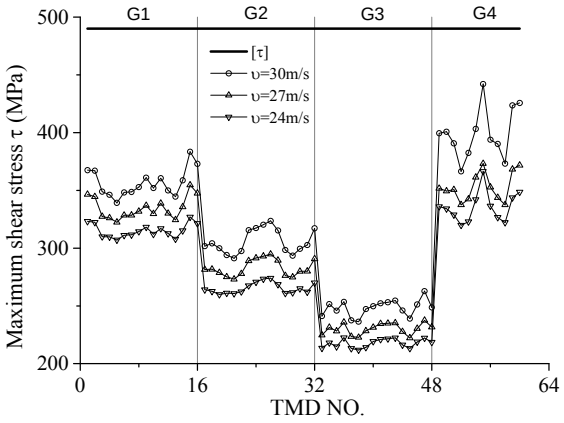

Fig. 14 Maximum shear stress of TMD springs wires at three levels of wind velocity

According to Fig. 14, the maximum shearing stresses of springs at three levels of wind velocity were smaller than $[\tau]$(490MPa), satisfying the usage requirement. As a result, the constraints brought by spring strength can be neglected during the optimization.

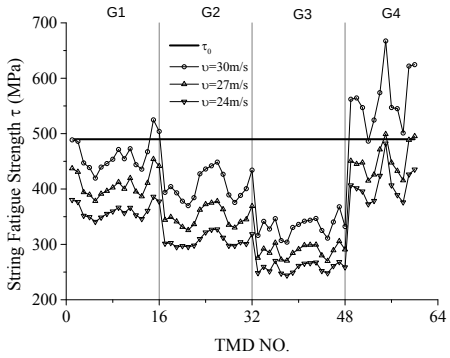

Fig. 15 Fatigue pulsation shearing stress of TMD spring wires at three levels of wind velocity

According to Fig. 15, the fatigue pulsation shearing stress of TMD springs at the wind velocity of 24m/s was smaller than τ_0 (490Mpa), which, however, increased with the increasing of wind velocity. When the wind velocity reached 27 m/s, the fatigue pulsation shearing stress of some TMD springs in G4 exceeded τ_0. Furthermore, when the wind velocity reached 30 m/s, the fatigue pulsation shearing stress of two TMD springs in G1 and all TMD springs in G4 exceeded τ_0. Therefore, some measures for preventing the TMD fatigue failure are demanded for satisfying usage of TMD.

6.3.3 Effect of spring constraints on the optimization results

Based on the analysis in Section 5.3.2, this part analyzed the effect of spring constraints under υ=30 m/s (basic wind pressure: 0.55 kPa) at 10m high above the ground on the MTMD optimization.

The optimized MTMD parameters when spring constraints were taken into account were listed in Table 9. The comparison between Tables 6 and 9 found that, when the TMD spring constraints were taken into account, different MTMD groups still maintained same frequency range and similar mass ratio. The damping ratio of G1 increased slightly, while the damping ratio of G2-G3 decreased slightly. However, the damping ratio of G4 increased from 7.83% to 18.51%, higher than its optimal damping ratio. The central tuning frequency ratios of all MTMD groups have some changes. G2 only decreased its central tuning frequency ratio by 0.009 and G3 decreased by 0.031. G1 is found to increase its central tuning frequency ratio significantly from 0.99 to 1.042 and G4 from 1.0 to 1.083, higher than their optimal central tuning frequency ratios.

From Table 9 it can be seen that, when the TMD spring constraints were taken into account, parameters of G4 changed the most significantly, followed by those of G1. Although parameters of G2 and G3 changed, they still remained within the optimal parameter range. It can be known from Fig. 15 that the fatigue pulsation shearing stress of TMD springs in G2 and G3 was smaller than the design requirement, which resulted in the slight change of their parameters. However, the fatigue pulsation shearing stress of two TMD springs in G1 exceeded the design limit, which resulted in some change of its damping ratio and central tuning frequency ratio. The fatigue pulsation shearing stress of all TMD springs in G4 exceeded the design limit and some TMD springs even exceeded significantly, which resulted in the great change of its damping ratio and central tuning frequency ratio.

Table 9 Optimized results of MTMD parameters considering constrains of TMD springs

NO. MTMD	mass ratio (μ)	damping ratio(ξ_T)	central tuning frequency ratio (λ)	frequency range (β) /Hz
G1	0.49%	11.90%	1.042	0.08
G2	0.40%	8.98%	1.058	0.08
G3	0.34%	8.33%	1.055	0.08
G4	0.37%	18.51%	1.083	0.08

Table 10 Reduction factors of P1-P4 nodes and mean reduction factors of G1-G4 considering the constrains of TMD springs

	P1	P2	P3	P4	G1	G2	G3	G4
Rwoc	39.89%	39.64%	34.77%	43.44%	40.95%	34.88%	28.62%	32.80%
Rwc	37.67%	38.29%	33.97%	36.76%	39.37%	34.42%	28.49%	29.72%

The reduction factors of optimized MTMD with or without spring constraints were listed in Table 10. R_{woc} represents the reduction factors without spring constraints and R_{wc} the reduction factors with spring constraints. When spring constraints were taken into consideration, the control effect of the MTMD decreased. The reduction factors of G1-G3 changed slightly, while the reduction factors of G4 changed significantly, decreasing by 15.4% for P4, 9.4% for G4. This is because when spring constraints were taken into consideration, the damping ratio and central tuning frequency ratio of G4 fell beyond its optimal range, which caused poorer behavior of G4.

The RMS of displacement of optimized TMDs with or without spring constraints were shown in Figs. 16-18 presented the maximum shearing stress and fatigue pulsation shearing stress.

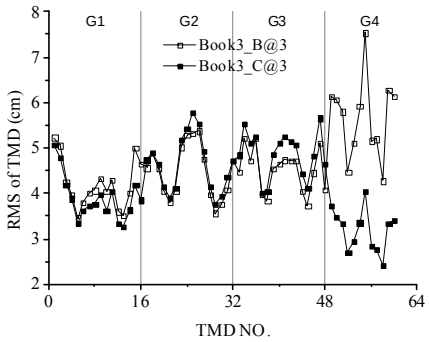

Fig. 16 RMS displacement of TMDs with / without considering the constrains of TMD spring

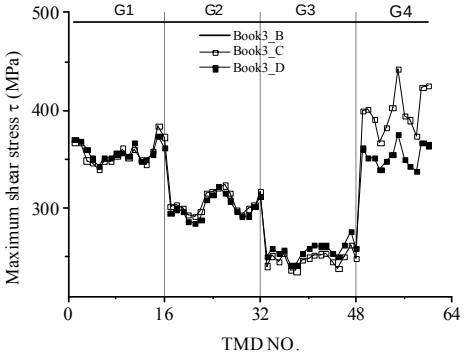

Fig. 17 Maximum shear stress of TMD spring wires with / without considering the constrains of TMD spring

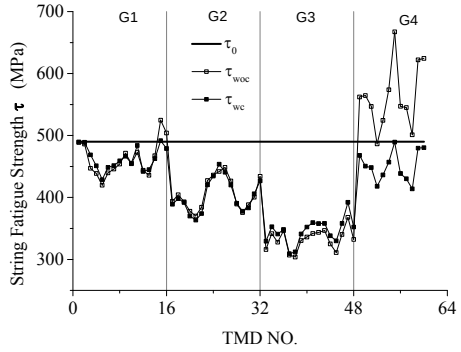

Fig. 18 Fatigue pulsation shearing stress of TMD spring wires with / without considering the constrains of TMD spring

According to Fig. 16, the RMS of displacement of TMDs in G2 and G3 with spring constraints was a little larger than that without spring constraints. This was due to the slight reduction of damping ratio. However, the RMS of displacement of TMDs in G1 and G4 with spring constraints was significantly smaller than that without spring constraints, especially that of G4. This was related with the increase of damping ratio. As shown in Figs. 17 and 18, the maximum shearing stress and fatigue pulsation shearing stress of the TMD springs in G1-G3 changed slightly no matter spring constraints were considered or not. However, the maximum shearing stress and fatigue pulsation shearing stress of the TMD spring in G4 decreased significantly when spring constraints were taken into account. Fig. 18 revealed that all springs have a satisfying the requirement of fatigue design.

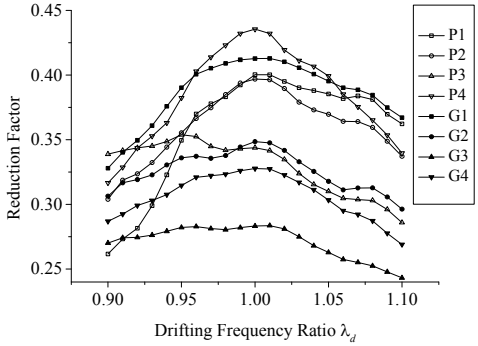

Fig. 19 Relationship between reduction factor and drifting frequency ratio

6.4 Robustness analysis

As an important index of TMD control system, robustness is used to evaluate whether the control effect of TMD changes significantly when the structural natural frequency drifts. The drifting frequency ratio was defined as,

$$\lambda_d = \frac{f_d}{f_s} \tag{16}$$

where, f_s is the original natural frequency of structure and f_d is the natural frequency after frequency drifting, which was ranging between $0.90 f_s$~$1.10 f_s$ for robustness analysis in this paper.

Fig. 19 represented the relationship between the reduction factors of P1-P4 and mean reduction factors of G1-G4 with the change of drifting frequency ratio. In Fig. 19, larger drift of structural natural frequency is accompanied with smaller vibration reduction factor of MTMD. When the structural frequency drifted, the structural natural frequency changed but MTMD was still designed according to the original natural frequency, thus resulting in the change of central tuning frequency ratio of MTMD. As stated before, MTMD has an optimal central tuning frequency ratio. Thus, larger difference between the central tuning frequency ratio and the optimal central tuning frequency ratio would cause poorer control effect.

When the drifting frequency ratio ranged between 0.9~1.1, the difference between the maximum and minimum reduction factors of P1-P4 was within 15%, and the difference between the maximum and minimum mean vibration reduction factors of G1-G4 was within 8%. This indicated that, the whole MTMD presented a good robustness, although the robustness of single node is relatively poor.

7. Conclusions

The optimization method of MTMD for large-span roof structures subjected to wind loads was established in the paper. The controlled modes and placements of TMDs in MTMD were

determined according to the modal contributions to the resonance component of wind-induced dynamic responses. To set reasonable boundary values of parameters for optimization, the parametric analysis, which focused on the effects of mass ratio, damping ratio, central tuning frequency ratio and frequency range of MTMD, was performed. Then through the genetic algorithms, the optimal parameters for MTMD were gained. Also, for purpose of engineering practice, the requirements of strength and fatigue life of TMDs spring were adopted as the constraint condition during the process of optimization.

The optimization method was applied to a specific shell structure. According to the selection principle, the controlled frequencies of MTMD for the structure were the natural frequencies of modes with maximum contributions to resonant component. The placement and number of TMDs were determined according to the key nodes with large displacement in the controlled modes. When the optimization did not involve the spring constraints, the reduction factors at some key nodes of the structure reached more than 34% and the mean vibration reduction factors more than 28%, which indicated the good control effect of the optimized MTMD. The study performed a preliminary investigation on the responses of TMDs spring under different wind velocities without involving spring constraints. The preliminary investigation showed that the fatigue pulsation shearing stresses of some TMD springs at higher level of wind velocity exceeded the shearing fatigue limit. Then the MTMD parameters were optimized when spring constraints were taken into account. While the requirements for strength and fatigue life of TMDs spring were considered, the MTMD had to satisfy the spring constraints at cost of control effect. The reduction factors at some key nodes changed significantly, decreasing by 15.4%. And some mean vibration reduction factors decrease by 9.4%. Finally, the robustness analysis was conducted in the study. When the drifting frequency ratio ranged between 0.9~1.1, the difference between the maximum and minimum reduction factors at some key nodes was within 15%, and the difference between the maximum and minimum mean vibration reduction factors was within 8%. This indicated that, the whole MTMD presented a good robustness.

Acknowledgments

This project is jointly supported by the National Natural Science Foundation (51278368, 51478359), and the Ministry of Science and Technology of China (SLDRCE14-B-10), which are gratefully acknowledged.

References

Abe, M. and Fujino, Y. (1994), "Dynamic characterization of multiple tuned mass dampers and some design formulas", *Earthq. Eng. Struct. D.*, **23**(8), 813-835.

Abe, M. and Igusa, T. (1995), "Tuned mass dampers for structures with closely spaced natural frequencies", *Earthq. Eng. Struct. D.*, **24**(2), 247-261.

Ahlawat, A.S. and Ramaswamy, A. (2003), "Multiobjective optimal absorber system for torsionally coupled seismically excited structures", *Eng. Struct.*, **25**(7), 941-950.

Avila, S.M. and Goncalves, P.B. (2009), "Optimal configurations of composite multiple mass dampers in tall buildings", *J. Brazilian Soc. Mech. Sci. Eng.*, **31**(1), 75-81.

Beasley, D., Martin, R. and Bull, D.(1993), "An overview of genetic algorithms: Part 1. Fundamentals", *University computing*, **15**, 58-58.

Carneiro, R.B., Avila, S.M. and De Brito, J.L.V. (2008), "Parametric study on multiple tuned mass dampers using interconnected masses", *Int. J. Struct. Stability Dynam.*, **8**(1), 187-202.
Carpineto, N., Lacarbonara, W. and Vestroni, F. (2010), "Mitigation of pedestrian-induced vibrations in suspension footbridges via multiple tuned mass dampers", *J. Vib. Control*, **16**(5), 749-776.
Chang, C.C., Gu, M. and Tang, K.H. (2003), "Tuned mass dampers for dual-mode buffeting control of bridges", *J. Bridge Eng.*, **8**(4), 237-240.
Chen, S.R., Cai, C.S., Gu, M. and Changrn, C.C. (2003), "Optimal variables of TMDs for multi-mode buffeting control of long-span bridges", *Wind Struct.*, **6**(5), 387-402.
Connor, J.J. (2003), *Introduction to structural motion control*, N.J., Prentice Hall Pearson Education, Inc..
Daniel, Y., Lavan, O. and Levy, R. (2012), "Multiple-tuned mass dampers for multimodal control of pedestrian bridges", *J. Struct. Eng. - ASCE* , **138**(9), 1173-1178.
Den Hartog, J.P. (1956), *Mechanical vibrations*, New York: McGraw-Hill.
Desu, N.B, Deb, S.K. and Dutta, A. (2006), "Coupled tuned mass dampers for control of coupled vibrations in asymmetric buildings", *Struct. Control Health Monit.*,**13**(5), 897-916.
GB/T 23935-2009 (2009a), *Design of cylindrical helical springs General Administration of Quality Supervision*, Inspection and Quarantine of the People's Republic of China, Standardization Administration of the People's Republic of China, SAC, , Standards press of China, Beijing.
GB 50009-2012 (2012), Ministry of Construction of the People's Republic of China, General Administration of Quality Supervision, Inspection and Quarantine of the People's Republic of China, Load code for the design of building structures, China Building Industry Press, Beijing.
Gu, M., Chen, S.R. and Chang, C.C. (2001), "Parametric study on multiple tuned mass dampers for buffeting control of Yangpu Bridge", *J. Wind Eng. Ind. Aerod.*, **89**(11-12), 987-1000.
Gu, M. and Xiang, H.F. (1992), "Optimization of TMD for suppressing buffeting response of long-span bridges", *J. Wind Eng. Ind. Aerod*., **42**(1-3), 1383-1392.
Hwang, J.S., Kim, H., Moon, D.H. and Park, H.G. (2011), "Control of floor vibration and noise using multiple tuned mass dampers", *Noise Control Eng. J.*, **59**(6), 652-659.
Jangid, R.S. and Datta, T.K. (1997), "Performance of Multiple Tuned Mass dampers for torsionally coupled system", *Earthq. Eng. Struct. D.*, **26**(3), 307-317.
Kareem, A. and Kline, S. (1995), "Performance of multiple mass dampers under random loading", *J. Struct. Eng. - ASCE*, **121**(2), 348-361.
Kwon, S.D. and Park, K.S. (2004), "Suppression of bridge flutter using tuned mass dampers based on robust performance design", *J. Wind Eng. Ind. Aerod.*, **92**(11), 919-934.
Lewandowski, R. and Grzymislawska, J. (2009), "Dynamic analysis of structures with multiple tuned mass dampers", *J. Civil Eng. Management* , **15**(1), 77-86.
Li, C.X. (2000), "Performance of multiple tuned mass dampers for attenuating undesirable oscillations of structures under the ground acceleration", *Earthq. Eng. Struct. D.*, **29**(9), 1405-1421.
Li, C.X. and Liu, Y.X. (2002a), "Further characteristics for multiple tuned mass dampers", *J. Struct. Eng. - ASCE*, **128**(10), 1362-1365.
Li, C.X. (2002b), "Optimum multiple tuned mass dampers for structures under the ground acceleration based on DDMF and ADMF", *Earthq. Eng. Struct. D.*, **31**(4), 897-919.
Li, C.X. and Zhu, B.L. (2006a), "Estimating double tuned mass dampers for structures under ground acceleration using a novel optimum criterion", *J. Sound Vib.*, **298**(1-2), 280-297.
Li, C.X. and Qu, W.L. (2006b), "Optimum properties of multiple tuned mass dampers for reduction of translational and torsional response of structures subject to ground acceleration", *Eng. Struct.*, **28**(4), 472-494.
Li, Q.A., Fan, J.S., Nie, J.G., Li, Q.W. and Chen, Y. (2010), "Crowd-induced random vibration of footbridge and vibration control using multiple tuned mass dampers", *J. Sound Vib.*, **329**(19), 4068-4092.
Lin, Y.J. (2013), *Wind-induced vibration control of large span roof structure with MTMD*, Master Dissertation, Tongji University, Shanghai.(written in Chinese)
Moon, K.S.(2010), "Vertically distributed multiple tuned mass dampers in tall buildings: performance analysis and preliminary design", *Struct. Des. Tall Spec.*, **19**(3), 347-366.

Mott, R.L.(2013), *Machine elements in mechanical design* (5th Edition). Publisher: Prentice Hall.
Nguyen, T.H., Saidi, I., Gad, E.F., Wilson, J.L. and Haritos, N. (2012), "Performance of distributed multiple viscoelastic tuned mass dampers for floor vibration applications", *Adv. Struct. Eng.*, **15**(3), 547-562.
Park, J. and Reed, D.(2001), "Analysis of uniformly and linearly distributed mass dampers under harmonic and earthquake excitation", *Eng. Struct.*, **23**(7), 13.
Patil, V.B. and Jangid, R.S. (2011), "Optimum Multiple Tuned Mass Dampers for the Wind Excited Benchmark Building", *J. Civil Eng. Management*, **17**(4), 540-557.
Singh, M.P., Singh, S. and Moreschi, L.M. (2002), "Tuned mass dampers for response control of torsional buildings", *Earthq. Eng. Struct. D.*, **31**(4), 749-769.
Ubertini, F.(2010), "Prevention of suspension bridge flutter using multiple tuned mass dampers", *Wind Struct.*, **13**(3), 235-256.
Wang, J.F. and Lin, C.C. (2005), "Seismic performance of multiple tuned mass dampers for soil-irregular building interaction systems" , *Int. J. Solids Struct.*, **42**(20), 5536-5554.
Warburton, G.B. (1982), "Optimum absorber parameters for various combinations of response and excitation parameters", *Earthq. Eng. Struct. D.*, **10**, 381-402.
Xu, K. and Igusa, T. (1992), "Dynamic characteristics of multiple substructures with closely spaced frequencies", *Earthq. Eng. Struct. D.*, **21**, 1059-1070.
Zheng, G., Ni, Y.Q., Li, H., *et al*. (2002), "Parameter optimization of multi-TMDs for wind-excited vibration suppression of tall buildings", *Adv. Build. Technol*., *Vols I and Ii, Proceedings*, 1025-1032.
Zhou, X.Y. and Gu, M. (2010), "An approximation method for computing the dynamic responses and equivalent static wind loads of large-span roof structures", *Int. J. Struct. Stability Dynam.*, **10**(5), 1141-1165.

CC